Supplementary Material for "Modelling a Dynamic Magneto-Agglutination Bioassay"

Robert Hughes, Aaron Fishman, Kathryn Lamb-Riddell,
Valentina Sleigh Muñoz, Alan Champneys, Janice Kiely and Richard Luxton

August 2022

S.1 Overview of the mathematical model

A flow diagram of the interconnecting sub-models is shown in Figure S.1. Each individual component of the model was described in outline in the each subsection of Section 5 in the main text and in more detail below. All the sub-model components were developed in Matlab.

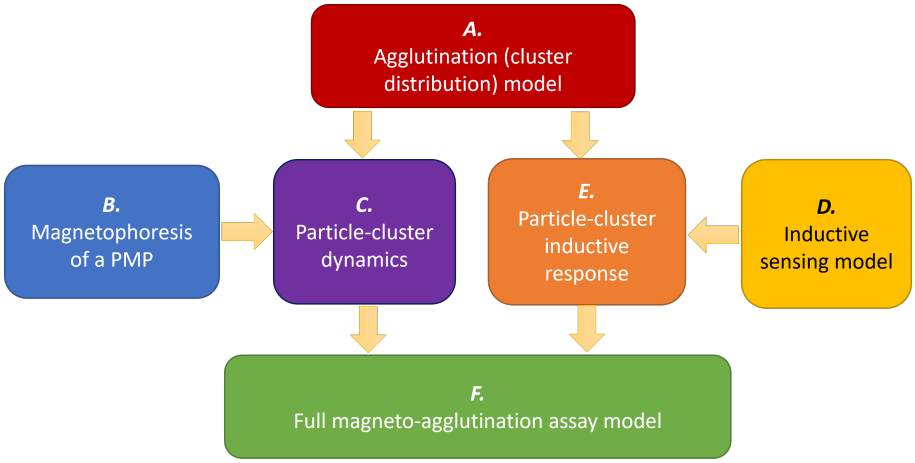

Figure S.1: Flow diagram of the interconnecting models: (A) dose-dependant agglutination clustering, using Becker-Döring theory; (B) magnetic force on an individual PMP; (C) dynamics of PMP clusters; (D) inductive sensor model; (E) inductive response to PMP clusters; (F) simulation model of the complete assay.

The main assumptions underlying our mathematical model can be summarised as follows.

1. Agglutination forms chain-like clusters of bacteria and PMPs. Although evidence shown in Section 2.6 suggests the clusters are more complex than this, it has been employed for simplicity of the model.

2. The assumed maximum number $N_{\max}$ of PMPs in a chain, is likely to be a large underestimate. One resolution is to think of a single model PMP as in truth representing a cluster of PMPs. Another point of view is to think that the only important output from the model is a realistic distribution of cluster sizes, in some arbitrary units of largest to smallest, as a function of bacterial dose.

3. All PMPs in a cluster occupy the same z-position i.e. experience the same B-field. This approximation is valid given the scale of clusters relative to the spatial change in magnetic flux density, and can be thought of as representing a cluster by its centre of mass, so that a cluster is equated to a single PMP with an effective radius of $r_{\text{eff}} = r_{\text{pmp}} \sqrt[3]{N}$.

4. In our model, clustering of PMPs does not affect the effective magnetic susceptibility, χ, of each PMP at a given B-field. While we believe this effect is likely to make little difference, more complex modelling would be required to quantify any necessary connection.

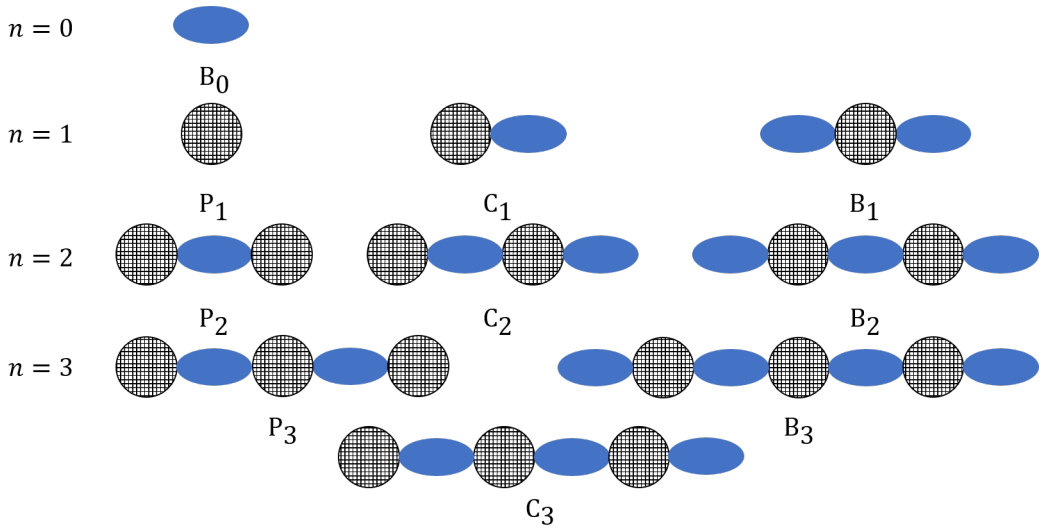

Figure S.2: The ten possible species types considered in an extended Becker-Döring equation model with up to three PMPs per cluster. The subscript number represents the number of PMPs in that species.

5. In the model, the PMP clusters are assumed to travel along a single straight line axially away from the inductive sensors. This is reasonable, given the sharp tunnel-like structure seen in in the experiments as the particles move (see Figure. 1.c), but full 3D modelling of trajectories could enable this assumption to be further tested.

6. The model simulates a magnet at rest at position $z = d$ (see Figures 4 & 2.b) at time $t = 0$, while $\mathbf{B_m} = 0$ when $t < 0$. In reality the magnet moves into position above the chamber, thereby introducing an increasing magnetophoretic force with time until coming to rest. This simplifying assumption is not likely to be particularly significant, and is a reasonable first guess without precise information on the magnets motion.

7. Magnetic self-assembly of 'naked' PMPs into larger structures (i.e. chains Messina, Khalil and Stankovic (2014)) in the presence of an external magnetic field is ignored. We believe this assumption is a likely dominant cause of error, especially at high magnetic field strengths. Essentially, our model assumes that clustering only occurs due to agglutination, and ignores this other mechanism for the formation of clusters. Nevertheless, the results in Fig. 3.b suggest this effect may have saturated at the concentrations of pmp/ml used. Future work will explore the relative importance of the two effects, in order to design an optimal operating point for the assay.

S.2 Becker-Döring equations for bacterial-PMP chain formation

The basic idea of the model is to produce a combinatorial set of rate equations for the creation of chains of length n, for n between 1 and some theoretical maximum N. Here we have adapted the usual Becker-Döring formalism system to allow for chain formation to occur via several separate steps, each of which occurs with a different assumed reaction rate (binding affinity); see Figure S.2. First, a free bacterium can bind to a chain that has two 'free' PMP ends. Alternatively, a bacterium can bind to a chain with a single free PMP. Also, a PMP can bind to a chain with either one or two bacteria at its end. Thus there are three different kinds of chains of n PMPs as depicted in Figure S.2 for $n = 0, \ldots, 3$.

One of the difficulties in quantitative comparison between model and experiment is to get reliable estimates for binding affinity. For simplicity in the model, we assume that the binding affinities for each of the steps depicted in Figure S.2 are equal. By making this assumption, we can assume a suitable rescaling of time so that we can run the model with a non-dimensional binding affinity of unity. The downside of such an assumption is that the time constant of the system to reach steady state will be unknown, without detailed information on the binding affinities.

This simple Becker-Döring-like model was extended to include the possibility of chains of length n_1 binding with chains of length n_2 for $n_{1,2} > 1$. Typically, such reactions will occur with a lower affinity

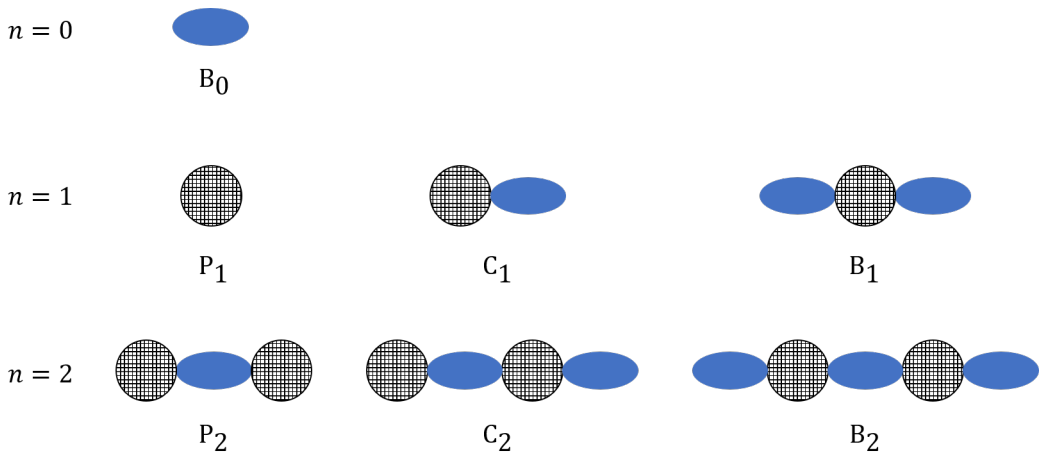

Figure S.3: The seven species types possible in the $N = 2$ chain model. The subscript number represents the number of PMPs in that species. Also, P_n represents a species containing one more PMP than bacteria, C_n represents a species containing an equal amount of bacteria and PMPs and B_n represents a species containing one more bacterium than PMPs.

than reactions that involve single PMPs or bacteria joining a chain, so we introduced a dimensionless parameter $\kappa > 0$ so that a reaction involving binding of chains of length $n = \min\{n_1, n_2\}$ is assumed to occur at rate $k/(1+n\kappa)$ where k is the rate of binding of the corresponding monomer (either a bacterium or a PMP). Intuitively $\kappa = 0$ means all reactions occur with equal probability where as $\kappa > 0$ means that longer chains bind with less probability than shorter ones.

Using the simple law of mass action kinetics, reaction-rate equations can be written down for the creating and destruction of each of the species B_n, C_n and P_n, as depicted in Figure S.2 for $n = 3$, for all $n \leq N$.

The fundamental principle of modelling chain formation is to use the law of mass action. In this model the value N represents the maximum number of PMPs in any one species type. The model follows some simple principles, but is moderately complex to write out in full. Therefore we shall adopt an approach of describing first the case where $N = 2$, in this case there would be six different species types as shown in Figure S.3. The number of different types of species for a certain value of N is therefore $3N + 1$.

S.2.1 The 2-chain model

Taking inspiration from the Becker-Döring model by Ball, Carr and Penrose (1986), it is assumed that a species that is neither B_0 or P_1 can only join to species B_0 or P_1, as B_0 and P_1 are acting as the monomer in the Becker-Döring equations. For example, if $N = 2$ the reaction equations are

$$B_0 + P_1 \xrightarrow{2k_1} C_1, \tag{S.1a}$$

$$B_0 + C_1 \xrightarrow{k_1} B_1, \tag{S.1b}$$

$$P_1 + C_1 \xrightarrow{k_2} P_2, \tag{S.1c}$$

$$P_1 + B_1 \xrightarrow{2k_2} C_2, \tag{S.1d}$$

$$B_0 + P_2 \xrightarrow{2k_1} C_2, \tag{S.1e}$$

$$B_0 + C_2 \xrightarrow{k_1} B_2, \tag{S.1f}$$

where the reaction rate constant for joining species B_0 to another species is k_1 and the reaction rate constant for joining species P_1 to another species is k_2. When there are two binding sites available for the B_0 or P_1 species to join to, the reaction rate constant is doubled. Also, note that it is assumed that reaction (S.1a) consists of adding the species B_0 to another species rather than the other way around. This assumption was made because bacteria are less dense so can move more quickly than the species P_1.

To turn the above chemical equations into differential equations for the concentration of each chemical species, we use the law of mass action. First though we non-dimensionlise so that $p_i(t)$, $b_i(t)$ and $c_i(t)$ represent the concentrations of p-type b-type and c-type species with respect to a given concentration scale and time scale. It is convenient to measure concentration with respect to the initial population of free PMPs, that is $p_1(0) = 1$, and to measure time so that $k_1 = 1$. This introduces two dimensionless parameters into the model: β which is ratio of initial concentration of b_0, divided by the initial concentration of p_1; and κ which is the ratio of k_1 to k_2. Note that β is a convenient parameter as it is effectively the dose of the target, whereas it is hard to gain quantitative information on κ. Nevertheless we found little qualitative change in our simulations as κ was varied, so all simulation results reported are for $\kappa = 1$.

Under these assumptions, the rate equations for the $N = 2$ chain model become

$$\frac{db_0}{dt} = -2b_0p_1 - b_0c_1 - 2b_0p_2 - b_0c_2, \tag{S.2a}$$

$$\frac{dp_1}{dt} = -2b_0p_1 - \kappa p_1c_1 - 2\kappa p_1b_1, \tag{S.2b}$$

$$\frac{dc_1}{dt} = 2b_0p_1 - b_0c_1 - \kappa p_1c_1, \tag{S.2c}$$

$$\frac{db_1}{dt} = b_0c_1 - 2\kappa p_1b_1, \tag{S.2d}$$

$$\frac{dp_2}{dt} = \kappa p_1c_1 - 2b_0p_2, \tag{S.2e}$$

$$\frac{dc_2}{dt} = 2\kappa p_1b_1 + 2b_0p_2 - b_0c_2, \tag{S.2f}$$

$$\frac{db_2}{dt} = b_0c_2, \tag{S.2g}$$

where $t_c = \frac{1}{k_1A}$ and $\kappa = \frac{k_2}{k_1}$.

Given that the total number of PMPs and bacteria must be conserved, these equations are subject to two constraints

$$b_0 = \beta - c_1 - 2b_1 - p_2 - 2c_2 - 3b_2, \tag{S.3a}$$

$$p_1 = 1 - c_1 - b_1 - 2p_2 - 2c_2 - 2b_2, \tag{S.3b}$$

which can be used to reduce the seven-dimensional system (S.2) to a five-dimensional system as necessary.

S.2.2 The general N-chain model

Using the model for $N = 2$ as a guide and following the same assumptions, the equations needed for any value of N can be determined. Firstly, it was deduced that there are only four possible different types of chemical step involving chains of length $n \leq N$, namely

$$\mathrm{B_0 + P_n \xrightarrow{2k_1} C_n} \qquad \text{for n} = 1 \ldots \text{N}, \tag{S.4}$$

$$\mathrm{P_1 + B_n \xrightarrow{2k_2} C_{n+1}} \qquad \text{for n} = 1 \ldots \text{N} - 1, \tag{S.5}$$

$$\mathrm{B_0 + C_n \xrightarrow{k_1} B_n} \qquad \text{for n} = 1 \ldots \text{N}, \tag{S.6}$$

$$\mathrm{P_1 + C_n \xrightarrow{k_2} P_{n+1}} \qquad \text{for n} = 1 \ldots \text{N} - 1. \tag{S.7}$$

For a particular value of n, there are three distinct cases, in order to calculate all of the non-dimensionalised rate equations. As before, $\kappa = \frac{k_2}{k_1}$.
Case 1: $0 \leq n \leq 1$. The first four rate equations are

$$\frac{db_0}{dt} = -\sum_{n=1}^{N} 2b_0 p_n - \sum_{n=1}^{N} b_0 c_n,$$

$$\frac{dp_1}{dt} = -2b_0 p_1 - (\sum_{n=1}^{N-1} 2\kappa p_1 b_n) - (\sum_{n=1}^{N-1} \kappa p_1 c_n),$$

$$\frac{dc_1}{dt} = 2b_0 p_1 - b_0 c_1 - (\kappa p_1 c_1),$$

$$\frac{db_1}{dt} = b_0 c_1 - (2\kappa p_1 b_1),$$

where the terms in brackets only occur when $N > 1$.
Case 2: when $2 \leq n \leq N - 1$ the next group of rate equations are

$$\frac{dp_n}{dt} = \kappa p_1 c_{n-1} - 2b_0 p_n,$$

$$\frac{dc_n}{dt} = 2\kappa p_1 b_{n-1} + 2b_0 p_n - b_0 c_n - \kappa p_1 c_n,$$

$$\frac{db_n}{dt} = b_0 c_n - 2\kappa p_1 b_n.$$

Case 3: for $n = N$ the last three rate equations are

$$\frac{dp_N}{dt} = \kappa p_1 c_{N-1} - 2b_0 p_N,$$

$$\frac{dc_N}{dt} = 2\kappa p_1 b_{N-1} + 2b_0 p_N - b_0 c_N,$$

$$\frac{db_N}{dt} = b_0 c_N.$$

Upon assuming that the total number of bacteria and PMPs are each conserved quantities, we get the following two constraints that can be used to eliminate two variables from the model:

$$b_0 = \beta - c_1 - 2b_1 - \sum_{n=2}^{N} \left((n-1)p_n + nc_n + (n+1)b_n\right), \tag{S.11a}$$

$$p_1 = 1 - c_1 - b_1 - \sum_{n=2}^{N} \left(np_n + nc_n + nb_n\right). \tag{S.11b}$$

Thus the system of $3N + 1$ rate equations is reduced to a system of $3N - 1$ rate equations.

The N-chain model system depends on parameters β, κ and N, in exactly the same way as the 2-chain model.

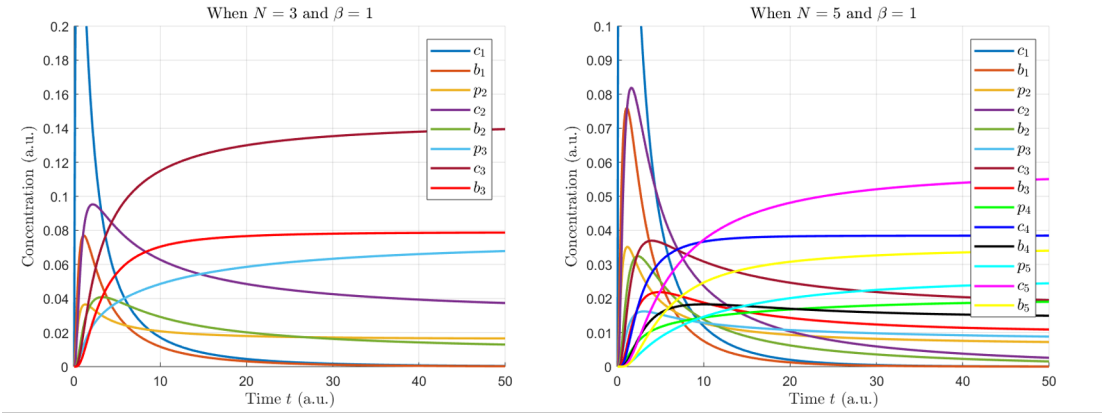

(a) (b)

Figure S.4: Results of an initial simulation of the extended N chain model with $\beta = 1$, $\kappa = 1$. (a) Illustrates when $N = 3$. (b) Illustrates when $N = 5$.

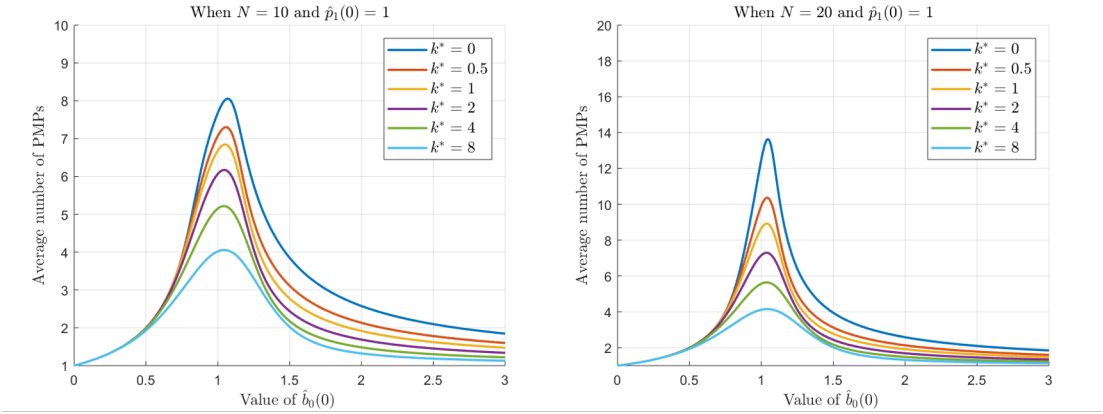

(a) (b)

Figure S.5: Dose-response curves (here $\hat{b}_0(0)$ on the horizontal axis is β) for varying values of κ with $T = 50$. (a) Illustrates when $N = 10$. (b) Illustrates when $N = 20$.

S.2.3 Model simulation results

The output from an example simulation is shown in Figure S.4. Intuitively, since forward reaction rates dominate reverse rates, one might expect that provided there are sufficient initial bacteria, then the model might 'run away' so that the steady state distribution is dominated by chains of maximum possible length, perhaps a single chain of length N. That this is not the case, can be understood from the conservation of total number of PMPs and bacteria. As longer chains are produced, so either bacteria or PMPs (whichever is not excess) are 'used up', leaving a tail of chains of smaller than maximal length.

Figure S.5 shows information on the final steady state reached measured by the mean cluster size, and as a distribution of cluster sizes. Here, we see a detailed shape of a dose response that rises rapidly, largely independently of the parameter κ, up to a peak value when the ratio β of target to PMP is 1. For excess target, the average cluster size decreases. While the peak reached is a function of the unknown parameter κ, we note that the response curve of cluster size versus β has the same characteristic shape in all cases. Moreover the size of the peak of this curve appears to scale approximately linearly with the maximum cluster size N — cf. panels (a) and (b) of Fig. S.5) which are for $N = 10$ and $N = 20$ respectively. Figure 4.c shows that in fact, the cluster sizes for β close to unity are actually widely distributed.

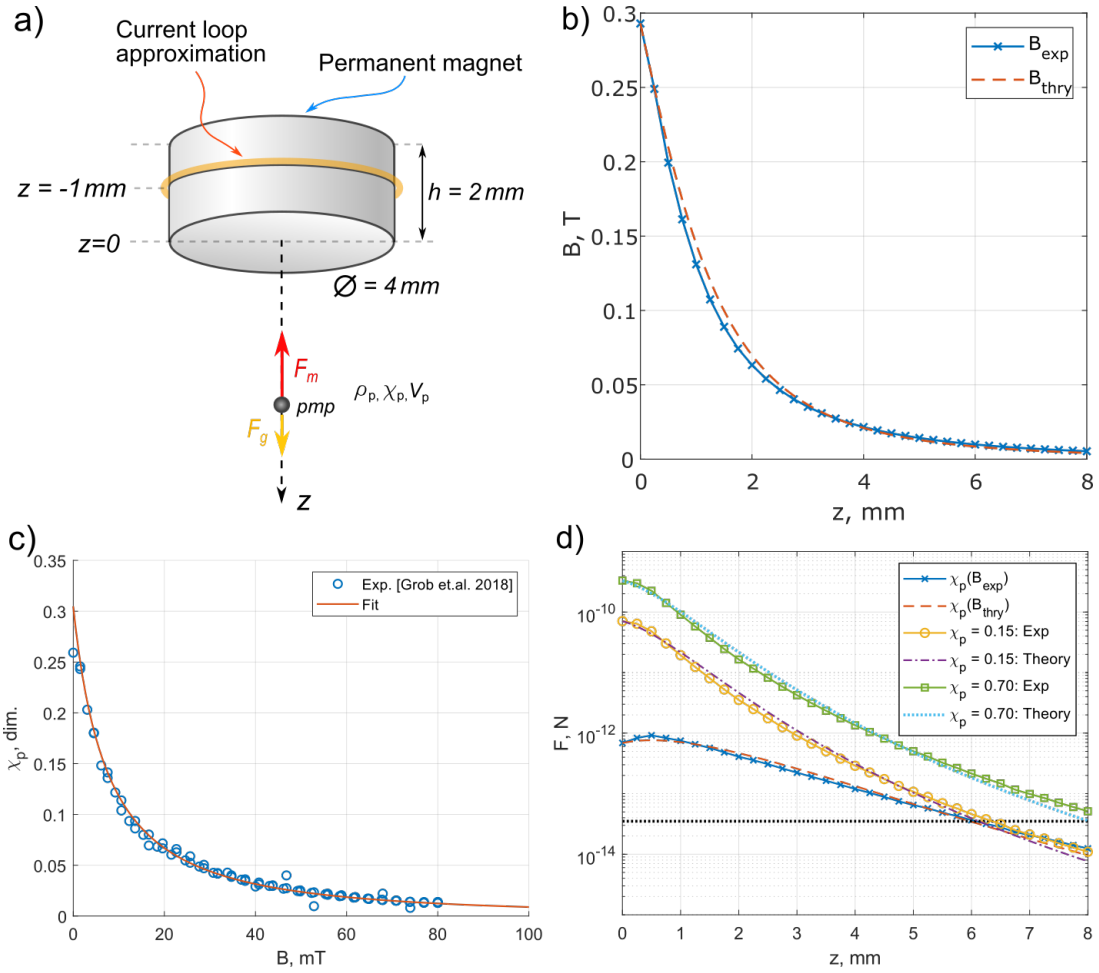

Figure S.6: Magnetophoretic force on a PMP. (a) The geometry of the magnetic field theoretical current loop model relative to the permanent magnet position. (b) The magnetic flux-density, $\mathbf{B}_m$, of the permanent magnetic used to perform magnetophoresis on PMP's showing experimental measurements compared to a Biot-Savart current loop model. (c) The experimentally measured magnetic susceptibility of 2.8 μm Dynabeads® as a function of the magnetic flux density, from Grob et al. (2018), along with a line of best. (d) The magnetic force acting on a PMP as a function of relative position to the face of the permanent magnet for different constant magnetic susceptibilities and the magnetic flux density dependant susceptibility from (c).

S.2.4 Magnetophoresis

We give here more details of the model developed in Section 5.2 of the main text.

S.2.4.1 Magnetic Flux Density B_m and Force F_m^p on a PMP

The magnetic flux-density of the permanent magnet was experimentally measured along it's z-axis (the vertical co-ordinate direction which separates the 'top' and 'bottom' of the chamber, which is also aligned with gravity) using a Hall-effect sensor. The results are shown in Fig. S.6 are compared to the simulated magnetic flux-density calculated using the Biot-Savart law for a current loop Griffiths (2008). The model can be expressed for a permanent magnet of height h and radius a, with its face located a distance d from the bottom of the assay chamber (i.e. $z = 0$) by the general form,

$$\mathbf{B}_m = \frac{B_0 a^3}{\left[(z - d_0)^2 + a^2\right]^{3/2}} \ \hat{\mathbf{z}}, \tag{S.12}$$

where a is the radius of the magnet/current-loop and B_0 is the magnetic flux density in the plane of the current loop (at $z = d_0 = d + h/2\ mm$). B_0 is calculated from the measured value at the surface of the

permanent magnet ($z = d\ mm$). This expression can be used to estimate the force on a single PMP, F_p^m Shevkoplyas, Siegel, Westervelt, Prentiss and Whitesides (2007),

$$F_p^m = \frac{V_p \Delta\chi}{\mu_0}(\mathbf{B_m} \cdot \frac{\partial}{\partial z})\mathbf{B_m}, \quad = 3\frac{V_p\,\Delta\chi}{\mu_0}\frac{{B_0}^2\,a^6\,(d-z)}{\left[a^2+(d-z)^2\right]^4}\,\hat{\mathbf{z}}, \tag{S.13}$$

where $\Delta\chi$ is the difference in magnetic susceptibility χ_p between the PMP and the surrounding medium, μ_0 is the magnetic permeability of free space and $\mathbf{B_m}$ is the magnetic flux-density of the permanent magnet. For the assay in question, the surrounding medium is a water-like fluid;whose magnetic susceptibility can be assumed to be negligible. But to create the final expression for the magnetic force on a PMP given in the main text, we need to estimate the the magnetic susceptibility χ_p of the particle.

S.2.5 Estimating magnetic susceptibility χ_p

In the literature, values for the magnetic susceptibility of 2.8 μm Dynabeads® ranges between 0.15-0.70 Fonnum, Johansson, Molteberg, Mørup and Aksnes (2005); Sinha, Anandakumar, Oh and Kim (2012); Grob et al. (2018). These bounds are shown in Fig. S.6.d, relative to the gravitational force, F_g, for the predicted magnetic force acting on a single PMP, calculated using (S.13). It predicts that the magnetic force acting on a single PMP of $\chi_p = 0.15$ will not overcome F_g if the PMP is more than 6 mm from the face of the permanent magnet, while a PMP of $\chi_p = 0.7$ will overcome F_g up to 8 mm. However, it is well-documented that χ_p is dependant on the applied magnetic field strength, and as such will vary as a function of z. Grob et al. (2018) provide experimentally measured B_m verse the magnetisation M curve data for 2.8μm Dynabeads® up to ±80 mT. This data was used to predict the susceptibility, $\chi_p = \mu_0\mathbf{M}/(\mathbf{B} - \mu_0\mathbf{M})$, as a function of $B_m(z)$ shown in Fig. S.6.c. A best fit was made to the data with the form,

$$\chi_p(z) = \frac{1}{c_1 B_m(z) + c_2} \tag{S.14}$$

where $c_1 = 4.30 \pm 0.04\ T^{-1}$ and $c_2 = 9.74 \pm 0.02$. Substitution of (S.14) into (S.13) leads to the form of F_p^m given in the main text (4).

S.3 Movement of PMPs in fluid under magnetic field

We suppose that a cluster of n PMPs and bacteria, formed by agglutination, can be represented by a buoyant sphere of volume V, radius R_n. We can use the theory of Stokes flow to calculate the forces acting on the entire cluster when in the testing chamber and under the effect of a magnetic field:

$$\rho_p V\ddot{z} = 6\pi\mu R_n\dot{z} + \Delta\rho V g + nF_p^m, \tag{S.15}$$

Here, drag force, calculated using Stokes' Law $F_d = 6\pi\mu R_n\dot{z}$ on a sphere of radius R_n moving through a fluid with a coefficient of dynamic viscosity μ at velocity $\dot{z}$ Stokes (2009). The density of a PMP is denoted ρ_p and the change in density between the surrounding fluid and the PMP by $\Delta\rho$. Also, g is the gravitational field strength on earth. See Fig. S.6(a).

The magnetic force experienced by a cluster of n PMPs is dependant on the volume of susceptible material (PMPs) present in the cluster; $F_c^m = nF_p^m$, with n being the number of PMPs in the cluster. Here we are assuming that the magnetic flux density is the same at all points across the cluster i.e. the cluster is very small in comparison to the flux density spatial decay.

Now, if we assume the total volume of the cluster is $V = nV_p$ where V_p is the volume of a single PMP and total radius $R_n = r_p n^{\frac{1}{3}}$ where r_p is the radius of a single PMP, substituting these terms into equation (S.15) leads to the following equation

$$\rho_p n V_p\ddot{z} = 6\pi\mu r_p n^{\frac{1}{3}}\dot{z} + \Delta\rho n V_p g + nF_p^m,$$

and by dividing by the number of PMPs in the cluster, n, the equation becomes

$$\rho_p V_p\ddot{z} = \frac{6\pi\mu r_p}{n^{\frac{2}{3}}}\dot{z} + \Delta\rho V_p g + F_p^m. \tag{S.16}$$

Table 1: Properties of Particle Dynamics Model

Name	Parameter	Value
PMP Susceptibility	χ_p	(see eqn S.14)
Susceptibility constant 1	α_1	$4.30 \pm 0.04 T^{-1}$
Susceptibility constant 2	α_2	$9.74 \pm 0.02 T^{-1}$
Fluid density	ρ_f	$1089 kg/m^3$
PMP density	ρ_p	$5240 kg/m^3$
PMP radius	r_p	$1.4 \mu m$
PMP Volume	V_p	$11.5 \times 10^{-18} m^3$
PMP Volume	V_p	$11.5 \times 10^{-18} m^3$
Fluid viscosity	μ	$0.8872 \times 10^{-3} Pa\ s$
Cluster size	n	$1 - 100$

Equation S.16 shows that only Stokes drag is dependent on the number of PMPs n. In particular as the cluster size n increases, the drag force decreases, and thus the terminal velocity must increase. As n increases the acceleration decreases but the velocity increases because of the force on the cluster due to the magnetic field. Thus, we can understand how mean velocity of particles depends on cluster size, which in turn depends on the concentration of target bacteria.

Finally, substitution of (4) into (S.16) gives a non-linear expression for the one-dimensional dynamics of a cluster of n PMPs,

$$\rho_p V_p \ddot{z} = \frac{6\pi\mu r_p}{n^{\frac{2}{3}}} \dot{z} + \Delta\rho V_p g + \frac{3}{2} \frac{V_p \chi_p}{\mu_0} \frac{B_0^2 a^6 (h + 2z)}{\left[(z + \frac{1}{2}h)^2 + a^2\right]^4}, \tag{S.17}$$

which has no analytical solution. Instead the system was solved numerically to give the trajectories, $z_n(t)$, of clusters of $1 \leq n \leq 100$ PMP's.

S.3.1 Inductive coil response

As stated in the main text, the magnetic flux density, $\mathbf{B_s}(r, z)$, generated by the coil is calculated via the linear summation of the field generated by each of the N_t coil turns carrying current I. Assuming each turn is the same width and there is a uniform distribution of current, we can approximate each turn as a series of M discrete filament turns (see Figure 4), with radius $a_{n_t,m}$, carrying a current $I_m = I/M$. The magnetic flux density at any location (r, z) above the coil can therefore be defined as the summation of the magnetic flux density contributions from each current carrying filament

$$\mathbf{B}_s(r, z) \approx \frac{\mu_0 I}{2\pi M} \sum_{n_t,m}^{N_t,M} \frac{\lambda_r \hat{\mathbf{r}} + \lambda_z \hat{\mathbf{z}}}{[z^2 + (r - a_{n_t,m})^2]\sqrt{z^2 + (r + a_{n_t,m})^2}}, \tag{S.18}$$

where

$$\lambda_r = \frac{z}{r}\left[\left(a_{n_t,m}^2 + z^2 + r^2\right) E_2(k) - E_1(k)\right],$$
$$\lambda_z = \left[\left(a_{n_t,m}^2 - z^2 - r^2\right) E_2(k) + E_1(k)\right],$$
$$k^2 = 4\frac{r a_{n_t,m}}{z^2 + (a_{n_t,m} + r)^2}.$$

Here $E_1(k)$ and $E_2(k)$ are elliptic functions of the first and second kinds respectively, and $\hat{r}$ and $\hat{z}$ are the radial and vertical unit vectors vector Gal-Katziri and Hajimiri (2019). Values of the various geometric constants are given in Table 2.

References

Ball, J., Carr, J., Penrose, O., 1986. The Becker-Döring cluster equations: Basic properties and asymptotic behaviour of solutions. Communications in Mathematical Physics 104, 657–692.

Fonnum, G., Johansson, C., Molteberg, A., Mørup, S., Aksnes, E., 2005. Characterisation of Dynabeads by magnetization measurements and Mössbauer spectroscopy. Journal of Magnetism and Magnetic Materials 293, 41–47.

Table 2: Properties of Inductive Magnetometer Model

Name	**Parameter**	**Value**
Inner radius	r_{in}	0.175 μm
Outer radius	r_{out}	1.75 mm
Turn Width	t_w	175 μm
Turn Depth	t_d	35 μm
Turn Pitch	Δa_n	35 μm
Number of turns	N_t	5
Number of unit elements per turn	M	5
Magnetic permeability of free space	μ_0	$4\pi \times 10^{-7} H/m$

Gal-Katziri, M., Hajimiri, A., 2019. Analysis and design of coupled inductive bridges for magnetic sensing applications. IEEE Journal of Solid-State Circuits 54, 1883–1894.

Griffiths, D., 2008. Introduction to Electrodynamics. Third ed., Pearson Benjamin Cummings.

Grob, D., Wise, N., Oduwole, O., Sheard, S., 2018. Magnetic susceptibility characterisation of superparamagnetic microspheres. Journal of Magnetism and Magnetic Materials 452, 134–140.

Messina, R., Khalil, L., Stankovic, I., 2014. Self-assembly of magnetic balls: From chains to tubes. Phys. Rev. E 89, 011202.

Shevkoplyas, S., Siegel, A., Westervelt, R., Prentiss, M.G., Whitesides, G., 2007. The force acting on a superparamagnetic bead due to an applied magnetic field. Lab on a Chip 7, 1294–1302.

Sinha, B., Anandakumar, S., Oh, S., Kim, C., 2012. Micro-magnetometry for susceptibility measurement of superparamagnetic single bead. Sensors and Actuators, A: Physical 182, 34–40.

Stokes, G., 2009. On the Effect of the Internal Friction of Fluids on the Motion of Pendulums, in: Mathematical and Physical Papers. Cambridge University Press, Cambridge, pp. 1–10. URL: https://www.cambridge.org/core/product/identifier/CBO9780511702266A006/type/book_part, doi:10.1017/CBO9780511702266.002.